Hard magnetic $Sm(Fe,Si)_9$ carbides: Structured and magnetic properties

L. Bessais, C. Djéga-Mariadassou, and A. Nandra
LCMTR, UPR209, CNRS, 2/8 rue Henri Dunant, Boîte Postal 28, F-94320 Thiais, France

M. D. Appay
Laboratoire de Réactivité de Surface, UMR7609, CNRS, Tour 54, Université Pierre et Marie Curie, 4 place Jussieu, F-75230 Paris Cedex 05, France

E. Burzo
Facultatea de Fizica, Universitatea Babes-Bolyai, 3400 Cluj-Napoca, Romania

(Received 13 June 2003; revised manuscript received 12 November 2003; published 12 February 2004)

The structural and magnetic properties of the metastable hexagonal $SmFe_{9-x}Si_xC$ compounds, where x is 0.25, 0.5, 0.75, and 1, have been investigated by means of powder x-ray diffraction, Curie temperature, magnetic moment and coercivity measurements, iron-57 Mössbauer spectroscopy, and high-resolution transmission electron microscopy. The Rietveld analysis points out a lattice expansion after carbon insertion. Upon carbonation the Curie temperatures are systematically 26 to 70 K higher than those of the homologous $Sm_2(Fe,Si)_{17}C_2$. The magnetic moment per iron atom increases with x but remains below that of the noncarbonated alloys. The statistical occupation of silicon in $3g$ site and the random distribution of the $2e$ dumbbell iron atoms have been taken into account to calculate the Wigner-Seitz cell volumes, which rule the hyperfine parameter assignment. The following sequence of isomer shift $\delta\{2e\}>\delta\{3g\}>\delta\{6l\}$ is used to deduce the following sequence of hyperfine field $H_{HF}\{2e\}>H_{HF}\{6l\}>H_{HF}\{3g\}$. From $Sm(Fe,Si)_9$ to their carbides, the increase of isomer shift is less pronounced for the $2e$ site with no carbon neighbor. The small volume effect on the weighted average isomer shift may indicate hybridization between $2p$ of carbon and $3d$ of iron stronger than that of nitrides. The best coercivity of 15 kOe is obtained for $SmFe_{8.75}Si_{0.25}C$ with annealing temperature of the noncarbonated powder at 750°C. However, $SmFe_{8.5}Si_{0.5}C$, with 13 kOe and an optimal grain size around 22 nm, presents a better thermal stability and might be suitable for permanent-magnet applications.

DOI: 10.1103/PhysRevB.69.064402 PACS number(s): 75.50.Bb, 75.50.Tt, 76.80.+y

I. INTRODUCTION

The basic principle of searching for permanent-magnet materials is as follows: combine an inexpensive transition metal with a sufficiently high Curie temperature and high magnetization with another component, such as a rare-earth element, in such a way that the resultant compound has a sufficiently high uniaxial magnetic anisotropy.

After the discovery of interstitial ternary $R_2Fe_{17}X$ alloys (R=rare earth, X=N or C) by Coey and Hong,[1] a new horizon was opened in magnetic materials. Besides the fundamental interest of such interstitial modified alloys, which revealed the fair agreement between experimental results and theoretical predictions based upon the expansion of the Fe-Fe distances, increasing the Fe magnetic moment and the Curie temperature, some of the alloys appeared as promising candidates for permanent-magnet applications. The introduction of interstitial atoms in the $R\bar{3}m$ Th_2Zn_{17}-type structure results in modification of the crystalline field potential and induces an enhancement of the anisotropy field, which turns uniaxial when the second-order Stevens coefficient of the rare earth is positive. Attention was then given to Sm_2Fe_{17} nitrides and carbides.

The interest of the carbides is their better thermal stability than that of nitrides.[2,3] Unlike the nitrides obtained only by gas-phase reaction, they can be produced by several routes such as conventional melting of appropriate amount of Sm and Fe-C prealloy,[4,5] arc-melting followed by melt-spinning,[6] gas-solid reaction of Sm_2Fe_{17} with hydrocarbon gas[2,7–10] or solid-state reaction by ball milling of Sm_2Fe_{17} blend and graphite and subsequent annealing[11] or mechanical alloying prior to gas-phase reaction.[12] Carbon insertion can be achieved with a significant improvement of the thermal stability by substitution for Fe by small amounts of $3p$ elements such as low-cost silicon, opening the route to high-temperature processes for the preparation of highly dense magnets.[7,9,10,13–17]

A large anisotropy field has been found previously on the $R\bar{3}m$ $Sm_2(Fe,Si)_{17}C$ alloys. The highest coercivities of these compounds, up to 8 kOe, were obtained from ribbons with conditions still maintaining the equilibrium $R\bar{3}m$ phase.[6] In this context, investigations on less studied out-of-equilibrium phases open the route to specifically improved intrinsic properties. Moreover, the out-of-equilibrium elaboration techniques may favor the adequate microstructure, consistent with better extrinsic magnetic properties. There are different processes for forming metastable phases. Mechanical alloying is one of the most convenient processes. The metastable 1/9 phase has been found to form in the mechanically alloyed materials after annealing at specific temperature. The competing processes of deformation, fracture, and welding continue during milling, resulting in composition changes and microstructural refinement. Subsequent annealing is ben-

eficial to the formation of metastable phases at relevant temperatures and even leads to the equilibrium phases at high temperatures.

It was shown recently that, on one hand, from x-ray diffraction investigations, the out of thermodynamic equilibrium $P6/mmm$ $Sm(Fe,Si)_9$ compounds are stable up to 800°C without any onset of extra lines belonging to the $R\bar{3}m$ structure. On the other hand, the noncarbonated $Sm(Fe,Si)_9$ alloys show Curie temperatures systematically just 30 K higher than those of the homologous Si-containing $R\bar{3}m$ $Sm_2(Fe,Si)_{17}$ alloys, with only a slight improvement of the magnetic moment per iron atom.[18,19]

The study of out-of-equilibrium carbonated $Sm(Fe,Si)_9$ alloys, to which no work has been devoted up to now, is the objective of this contribution. The structure, intrinsic magnetic properties such as Curie temperature, magnetic moment, and hyperfine parameters will be reported on $Sm(Fe_{9-x}Si_x)$ alloys high-energy ball-milled and subsequently annealed, carbonated with a solid-state reaction by means of heavy hydrocarbon.[20] Owing to the samarium neutron absorption, Mössbauer spectroscopy appears to be the powerful corroborative technique to understand these out-of-thermodynamic equilibrium phases. Finally, the effect of annealing temperature upon microstructure and coercivity will be reported and discussed on the basis of high-resolution transmission electron microscopy experiments combined with energy dispersive x-ray analysis.

II. EXPERIMENT

Polycrystalline $Sm(Fe_{9-x}Si_x)$ alloys ($x=0.25,0.5,0.75,1$) were obtained by ball milling an appropriate stoichiometric mix of Sm_2Fe_{17}, Si (99.99%) and Sm (99.9%) powders. The Sm powder was weighed in with an excess of 12% in order to maintain a Sm overpressure on the sample. The quality of Sm_2Fe_{17} prealloy was checked by inductively coupled plasma atomic emission spectroscopy. Milling was performed for 5 h under high-purity Ar atmosphere with a ball to powder ratio of 15:1 as explained previously.[21] These milling conditions correspond to kinetic shock energy, shock frequency and injected shock power values, respectively, equal to 0.81 J/hit, 62 Hz, and 19.5 W/g.[22] The samples wrapped in tantalum foil were annealed for 30 min under vacuum at 750°C for $x=0.25$ and 0.5, at 850°C for $x=0.75$ and 1 according to the conditions established previously, consistent with a pure hexagonal phase.[19] However to study the evolution of coercivity, annealing for 30 min between 650 and 1150°C has been performed.

Carbonation was achieved after reacting $Sm(Fe_{9-x}Si_x)$ powders ground to 50 μm with an appropriate amount of $C_{14}H_{10}$ powders. In the known $Sm_2(Fe,Si)_{17}$ $R\bar{3}m$ alloys, most of the works are related to a carbon nominal composition of two atoms per formula unit although from a crystallographic point of view, a carbon content up to three atoms can be reached. It had been observed indeed that additionally carbonized alloys do not show any further Curie temperature enhancement.[6–8] The link between homologous alloys $R\bar{3}m$ $Sm_2(Fe_{1-y}Si_y)_{17}C_2$ and $P6/mmm$ $Sm(Fe_{1-x}Si_x)_9C$ is based upon the same relative Si content given by the relationship between x and y, i.e., $y=x(17/9)$. In order to get a similar relative nominal carbon stoichiometry per unit formula, we have prepared the series $Sm(Fe_{9-x}Si_x)C$. The mixtures of alloys and $C_{14}H_{10}$ were annealed at 420°C under vacuum for 48 h to ensure a good homogeneity of the carbon distribution. Mg chips inside the reacting tube absorbed the hydrogen overpressure resulting from the cracking of the hydrocarbon.[23]

X-ray diffraction measurements were carried out with Cu $K\alpha$ radiation on a Bruker diffractometer equipped with a single crystal monochromator. An internal Si standard was used to ensure a unit-cell parameter accuracy of $\pm 1\times 10^{-3}$ Å. Intensities were measured from $2\theta=20$ to 100 deg with a step size of 0.04 deg and counting time of 22 s per scanning step. The data were fitted by the Rietveld technique using the FULLPROF computer code in the assumption of Thompson-Cox-Hastings line profile which permits the refinement of each of the coexisting phases and takes into account the broadening of the diffraction lines induced by grain size and strain effects. The classical goodness-of-fit agreement factors χ^2 and R_B have been used.[24–27]

The Curie temperatures T_C were measured on a differential sample magnetometer (MANICS) in a field of 1000 Oe, with around 10 mg sample sealed under a vacuum in a small silica tube in order to prevent oxidation during heating. Magnetization measurements were performed with a vibrating-sample magnetometer at 4 K with applied field up to 90 kOe. Hysteresis loops were obtained at room temperature with a maximum applied field of 17 kOe (MANICS) or 55 kOe (superconducting quantum interference device).

The ^{57}Fe Mössbauer spectra were collected at room temperature using a constant-acceleration 512-channel spectrometer working in the mirror image mode with a 50 mCi ^{57}Co in Rh source and absorbers containing 12 mg of natural iron per cm^2. The α-iron reference had a full width at half maximum of 0.25 mm/s for the external peaks. The spectra were least-square fitted assuming Lorentzian lines without thickness broadening of the absorption lines. The estimated errors are ± 1 kOe for hyperfine field H_{HF}, ± 0.005 mm/s for isomer shift δ, and quadrupole interaction 2ϵ.

High-resolution transmission electron microscopy (HRTEM) was performed in bright field mode. The instrument used was a JEOL 2010 operating at 200 kV. The sample powders were embedded in epoxy and ultrathin sections (ca. 70 nm thick) were photographed at a magnification from 40 000 to 800 000. Interfringe measurements were performed and confirmed by Fourier-transform images obtained with local software on digitized negatives. A systematic energy dispersive x-ray analysis was carried out for each experiment with a spot size of 10 nm in order to *in situ* verify the nature of observed species.

III. RESULTS AND DISCUSSION

A. Structure analysis

The x-ray diagrams of the $Sm(Fe,Si)_9C$ series (Fig. 1) show a major phase (around 97 wt %) typical of the hexagonal $P6/mmm$ $SmFe_9$ structure as obtained previously, with

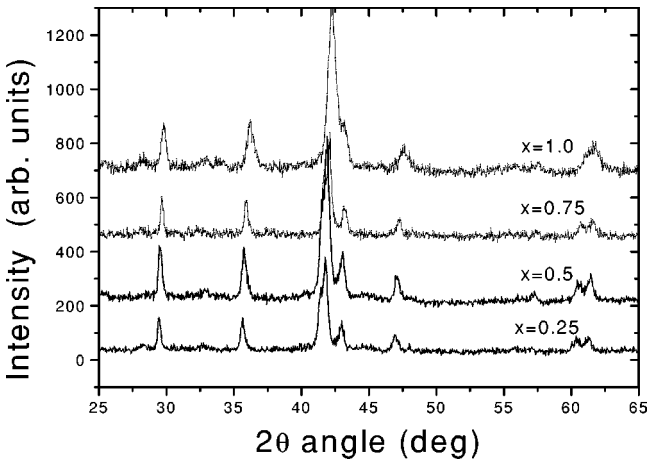

FIG. 1. X-ray diagrams of $SmFe_{9-x}Si_xC$.

shifted line positions compared to the noncarbonated alloys.[19] Small amounts of Sm_2O_3 are detected. Sm_2O_3 is logically assigned to the initial excess of Sm. It reacts with traces of oxygen still present on the reacting powder surface or with air during the measurements. α-Fe is only observed for $SmFe_{8.75}Si_{0.25}C$. It may result from a small decomposition of the $Sm(Fe,Si)_9$ phase occurring during the carbonation process because no α-Fe was observed, neither on the x-ray diagram nor on the Mössbauer spectra before carbonation.[19] This Fe amount, more accurately detected by ^{57}Fe Mössbauer spectroscopy as explained below, disappears with x increasing. This result gives evidence for the benefit effect of Si upon the thermal stability of the $P6/mmm$ phase.

Presence of higher amount of α-Fe has been observed in all works concerning the carbonation of the $R\bar{3}m$ 2/17 Sm-Fe phase, whatever the substituting element Si, Ga, Al and the carbonation process.[3,6,7,9–11,13,15,17]

The lattice parameters of the $Sm(Fe,Si)_9C$ alloys were determined from the corresponding Rietveld refinements for their nominal composition, according to the atomic distribution used previously to describe the $P6/mmm$ unit cell of the noncarbonated alloys with one C randomly distributed over all three $3f$ positions $(\frac{1}{2},0,0),(0,\frac{1}{2},0),(\frac{1}{2},\frac{1}{2},0)$. The location of the carbon atom is deduced from its counterpart's location in the $R\bar{3}m$ $Sm_2(Fe,Si)_{17}$ structure. The unit-cell parameter evolution with Si increasing reflects the same trend as that of the noncarbonated samples, just less pronounced. For the smallest Si content up to $x=0.5$, $\Delta a/a$ per Si atom is equal to -0.26% while c remains constant within the experimental uncertainty. From $x=0.75$ to 1, $\Delta a/a$ is negative equal to -0.45% and $\Delta c/c$ positive equal to $+0.40\%$. These unit-cell parameter evolutions corroborate the small iron enrichment of the $SmFe_9$ phase yet evidenced previously on the noncarbonated alloys,[19] supported by the model proposed by Buschow and Van der Goot.[28]

Upon carbonation for a given Si content, the unit-cell volume increases; but versus silicon content, this increase is reduced. The results of the structure refinement performed for the carbonated alloys are listed in Table I with 0.72–0.76 Fe atom in $2e$ $(0,0,Z)$ position, 2 Fe atoms in the $6l$ position $(X,2X,0)$ and the $3g$ site $(\frac{1}{2},0,\frac{1}{2})$ occupied totally by Fe and Si according to the Si content. The samarium site (0,0,0) is occupied by 0.64–0.62 atom within the scheme $Sm_{1-s}(Fe,Si)_{5+2s}$.[19] As an example, Fig. 2 illustrates the Rietveld plot for $SmFe_{8.75}Si_{0.25}C$.

TABLE I. a,c cell parameters, and R_B,χ^2 factors from the Rietveld fit for $SmFe_{9-x}Si_xC$.

	$x=0.25$	$x=0.5$	$x=0.75$	$x=1$
a (Å)	5.024	5.011	4.990	4.965
c (Å)	4.196	4.197	4.212	4.213
V (Å^3)	91.715	91.220	90.835	89.931
$\Delta V/V$ (%)	5.05	4.75	4.43	3.75
D (Å)	214	193	181	169
Strain rate (%)	0.722	0.830	0.862	0.903
R_B	3.89	4.99	5.89	5.33
χ^2	1.66	1.22	2.17	2.19
$X\{6l\}$	0.285	0.286	0.287	0.285
$Z\{2e\}$	0.284	0.286	0.290	0.294
T_C (K)	690	675	667	654
μ (μ_B/Fe)	1.45	1.51	1.72	1.75

The Rietveld refinements lead to an evaluation of the autocoherent diffraction domain size of 22 nm with a strain rate of 0.7% for $x=0.25$. They decrease slightly to 18 nm for $x=1$ according to the role played by Si on the microstructure. It slackens the grain coarsening but increases the strain rate (Table I).

B. Intrinsic magnetic properties: Curie temperature and magnetic moments

For comparison, homologous compounds $Sm_2(Fe_{1-y}Si_y)_{17}C_2$ with ordered $R\bar{3}m$ structure have been prepared according to the same process as that for the $Sm(Fe_{1-x}Si_x)_9C$ (the relationship between x and y is $y=x\times 17/9$) alloys but they were annealed before carbonation at 1150°C.

Figure 3 reports the Curie temperature evolution versus Si content for the noncarbonated and carbonated 1/9 alloys and

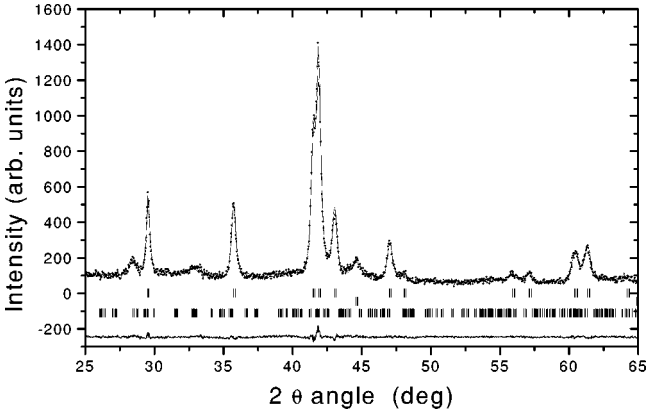

FIG. 2. Rietveld analysis of $SmFe_{8.75}Si_{0.25}C$. The set of ticks refer, respectively, to $SmFe_{8.75}Si_{0.25}C$, α-Fe, and Sm_2O_3.

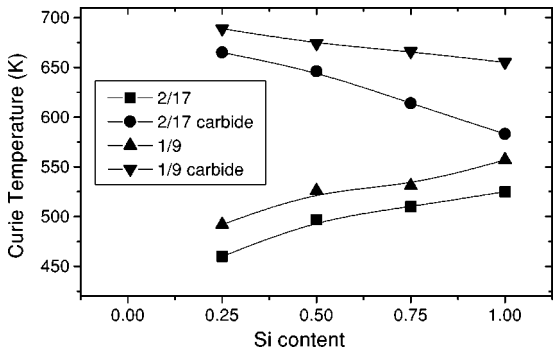

FIG. 3. Curie temperature vs Si content x for $P6/mmm$ and $R\bar{3}m$ phases and their carbides.

their homologous compounds 2/17 with, respectively, the $P6/mmm$ and the ordered $R\bar{3}m$ structure. The carbonated samples exhibit Curie temperatures above the noncarbonated ones in agreement with the known magnetovolumic effect (Table I). Moreover the Curie temperatures of the carbonated $P6/mmm$ alloys are systematically higher than those of the carbonated $R\bar{3}m$ series, 26 deg for $x=0.25$ up to 70 for $x=1$ in agreement with the results observed on the noncarbonated alloys.[18,19]

The average magnetic moment per Fe atom at 5 K (Table I) has been calculated from the magnetization value obtained at 90 kOe on the assumption of free-ion moment for samarium. The moments given in Table I are not saturation values. It appears smaller than that concerning the noncarbonated alloys. It increases with Si content from $1.45\mu_B$ up to $1.75\mu_B$ per Fe atom, respectively, for $x=0.25$ and 1 while for the noncarbonated alloys, it was found to increase from $1.88\mu_B$ to $1.97\mu_B$ per Fe atom for the same Si content. The smaller values of the magnetic moment of the carbonated samples agree with the fact that they are hard magnetic materials. The moment increase with x, consistent with the asymmetric filling of the iron $3d$ band by the silicon $3p$ electrons,[29] yields a reduction of the anisotropy field.

C. Hyperfine parameters

The experimental and fitted Mössbauer spectra are reported as a function of x in Fig. 4. Their analysis takes into account the presence of a possible α-Fe contribution besides the main $Sm(Fe_{1-x}Si_x)_9C$ as suggested by x-ray analysis. The amount of Fe equal to 8% wt for $x=0$ decreases to 6% wt for $x=0.25$ and is not detected for $x=0.5$. These results are deduced from the percentage increase of the Fe absorption lines upon a weighted Fe addition. This result corroborates the stabilizing effect of Si.

The interpretation of the spectra relative to the $P6/mmm$ phase is based on the counting of the various iron neighbors in the assumption of a binomial atom distribution law and on the assignment of the hyperfine parameter sets $\delta, H_{HF}, 2\epsilon$ to the various crystalline sites according to the relationship between the isomer shift δ and the Wigner-Seitz cell (WSC) volumes: the larger the WSC volume, the larger the isomer shift.[18–21] The WSC volumes have been calculated by means of Dirichlet domains and coordination polyhedra for each

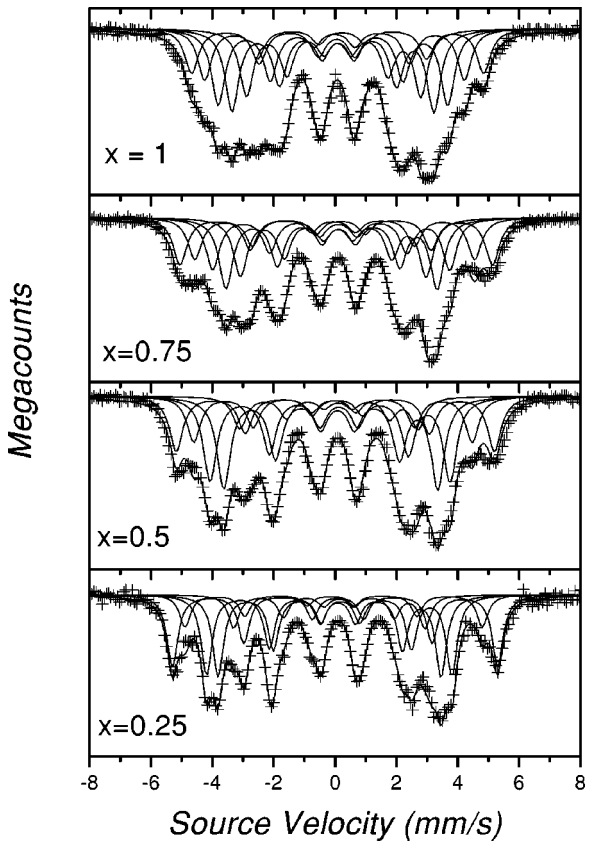

FIG. 4. The room-temperature Mössbauer spectra of hexagonal $Sm(Fe_{1-x}Si_x)_9C$.

crystallographic family $2e$, $3g$, $6l$, and $3f$ with radius values[30] of 1.81, 1.26, 1.17, and 0.70 Å for, respectively, Sm, Fe, Si, and C. The statistical occupation of Si in the $3g$ site and the random distribution of the $2e$ dumbbell atoms have been simulated by the use of an appropriate $P6/mmm$ subgroup, $P1$ with $a'=3a$, $b'=3a$, $c'=2c$ ($V'=18V$), allowing the splitting of the partially Si occupied positions according to the procedure used for the noncarbonated samples (Si randomly distributed over 54 positions). The WSC volumes calculated with the crystallographic parameters given in Table I are reported in Table II. The following sequence for the WSC volumes ($2e>3g>6l$) is obeyed whatever the Si content, but all values decrease versus x just as the unit-cell volumes.

The somewhat large width of the Mössbauer spectrum carbide contribution (Fig. 4) remains the same as that of $Sm(Fe,Si)_9$, Ref. 19, and originates likely from the statisti-

TABLE II. Wigner-Seitz cell volumes (Å^3) in $SmFe_{9-x}Si_xC$, $P6/mmm$.

x	Sm{1a}	Fe{2e}	Fe{3g}	Fe{6l}
0.25	34.76	20.68	13.74	13.65
0.5	34.68	20.60	13.68	13.53
0.75	34.36	20.29	13.50	13.42
1	33.96	19.87	13.45	13.39

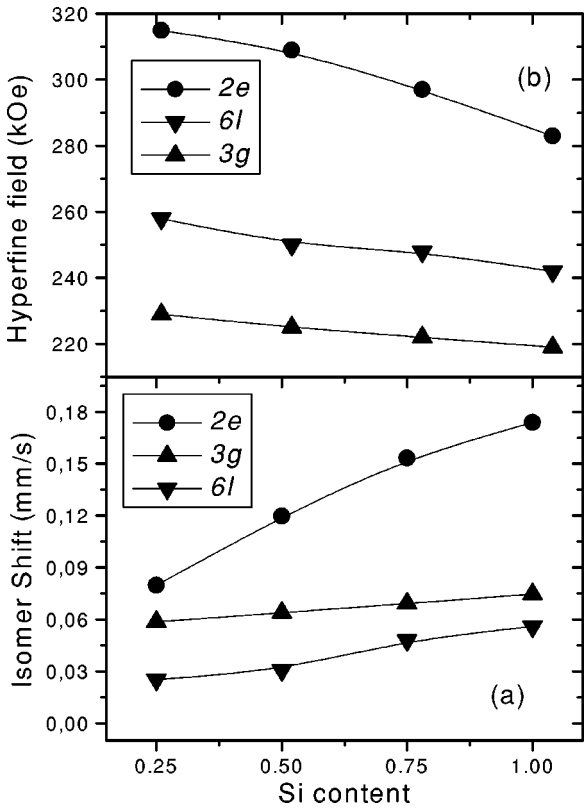

FIG. 5. The compositional dependence of (a) the isomer shifts and (b) the hyperfine fields for the $Sm(Fe_{1-x}Si_x)_9C$. The plotted data are the weighted average values for the three sites.

cal occupancy of silicon over the $3g$ sites. This behavior indicates that the possible disorder introduced by carbon insertion in the lattice or by an incomplete carbon filling of the $3f$ sites plays a second role.

The compositional dependences of isomer shift and hyperfine field are shown, respectively, in Figs. 5(a) and 5(b) for the three iron sites.

The mean hyperfine field decreases with Si content as observed in the $P6/mmm$ $Sm(Fe,Si)_9$ and in the $R\bar{3}m$ $Sm_2(Fe,Si)_{17}$ compounds. It results from the competition between the negative core polarization term and the positive term arising from $4s$ conduction electrons. The following hyperfine field sequence $H_{HF}\{2e\}>H_{HF}\{6l\}>H_{HF}\{3g\}$ is obtained. This classification matches closely the number of iron near neighbor of each site (Tables III and IV).

As an example, for $x=0.25$, the increase of $2e$, $6l$, and $3g$ hyperfine fields by 34, 25, and 10 kOe at room temperature after carbonation is related to the increase of the Curie temperature from about 492 to 689 K.

The isomer shift behavior with Si content at 293 K is reported in Fig. 5(a). For a given x value, the relation $\delta\{2e\}>\delta\{3g\}>\delta\{6l\}$ is always obeyed, according to our assumption derived from the WSC volumes. The mean isomer shift of the $2e$ and $6l$ atoms increases upon Si substitution, while it remains quasiconstant for the $3g$ atoms. This behavior corroborates the preferential occupation of silicon atoms at this site as found in Ref. 19.

TABLE III. Interatomic distances in the hexagonal $P6/mmm$ structure for $SmFe_{9-x}Si_xC$ ($x=0.25$, as an example, $a=5.024$ Å, $c=4.196$ Å). The distances are calculated inside a radius of the coordination sphere equal to 2.76 Å.

Fe sites	Distance (Å)	Number of of neighboring atomic sites	Average number of Fe neighbors	C,Fe,Fe/Si
$6l$	1.29	2	6.89	$3f$
	2.46	4		$3g$
	2.48	2		$6l$
	2.75	2		$2e$
	2.75	2		$3g$
$2e$	2.39	1	7.86	$2e$
	2.67	6		$3g$
	2.75	6		$6l$
$3g$	2.10	2	5.73	$3f$
	2.46	4		$6l$
	2.51	4		$3g$
	2.67	2		$2e$

The isomer shift is affected by the presence of the interstitial element. Going from $Sm(Fe,Si)_9$ to their carbides we have noticed an increase of the isomer shift for each crystallographic site. The increase of isomer shift ($\Delta\delta$) reflects the decrease of electron density with carbon insertion.

It indicates that the combined effect of volume expansion and charge transfer from the rare-earth $6s$ orbital to the carbon atoms is quite significant. This means that the interstitial element in the $P6/mmm$ crystal structure induces a modification of the rare-earth $6s$ orbital. This is not surprising because the interstitial elements act as first neighbors of the rare earth. In addition the short bonds observed between Sm and the interstitial atom witness hybridization. The increase is more pronounced in the case of $3g$ ($\Delta\delta\{3g\}=0.037$ mm/s) and $6l$ sites ($\Delta\delta\{6l\}=0.062$ mm/s) than for $2e$ ($\Delta\delta\{2e\}=0.029$ mm/s). Fe atoms at the $2e$ site have no C near neighbor. It might explain the smaller increase in $\Delta\delta$ observed at this site upon carbonation.

The expansion of the lattice induces the well-known volume effect on the weighted average isomer shift ($\overline{\delta}$). The decrease of the electron density at the iron nucleus produces an increase in the observed weighted isomer shift $\Delta\overline{\delta}$ of 0.05 mm/s. This value is lower than the value 0.12 mm/s reported by Hu *et al.*[31] for nitrides, although their volume expansion is similar ($\sim 5\%$) The volume effect on the iron isomer shift $\Delta\overline{\delta}/\Delta(\ln V)$ is typically 1.3 mm/s for close-packed structure;[32] the value obtained for $Sm(Fe,Si)_9C$ in this work is 0.9 mm/s, whereas the value of the nitrides[31] is 1.8 mm/s. One possible interpretation is that interband charge transfer between $3d$ and $4s$ occurs in the opposite sense in nitrides and carbides. Another possibility is a greater $4s$ $2p$ interatomic charge transfer in the nitrides, on account of the greater electronegativity of nitrogen. According to band calculations on $Y_2Fe_{17}X_3$ (X=C,N) Ref. 33, the hybridization between $2p$ of carbon and $3d$ of iron is stronger than that of nitride, which decreases the magnetic moment of carbide

TABLE IV. Mössbauer hyperfine parameter for $SmFe_{8.75}Si_{0.25}C$, as an example, at room temperature. Hyperfine field, H_{HF} (kOe); isomer shift, δ (mm/s); quadrupole interaction, 2ε (mm/s), and relative area, A (%). Linewidth $\Gamma = 0.32$ mm/s.

	$2e_0$	$2e_1$	$\langle 2e \rangle$	$3g_0$	$3g_1$	$\langle 3g \rangle$	$6l_0$	$6l_1$	$\langle 6l \rangle$
H_{HF}	317	300	315	228	236	229	263	220	258
δ	0.060	0.061	0.061	0.018	0.046	0.043	0.020	0.010	0.018
2ε	0.062	0.020		−0.015	−0.039		−0.105	−0.106	
A	12.6	1.4	14.0	44.4	10.0	54.4	24.5	7.0	31.5

more than in the nitride and may weaken the screening effects of *d* electrons of iron on the carbide more than on the nitride.

D. Coercivity

Figure 6 shows the hysteresis loop for $SmFe_{8.75}Si_{0.25}C$ as an example. Figure 7 represents the coercive fields H_C measured at 55 kOe for $x = 0.25$, 0.5, 0.75, and 1 versus the annealing temperature T_A of the as-milled powders before carbonation. For annealing temperatures higher than 1000 °C, the structure becomes $R\bar{3}m$. The maximum coercive field of 15 kOe is reached for the alloy $x = 0.25$, annealed at 750 °C. The maximum seems to shift towards 800 °C for all remaining alloys. They are, however, described by the $P6/mmm$ space group. The H_C value is still high, around 13 kOe for $x = 0.5$ but decreases down to 8.5 kOe for $x = 1$. This variation can be correlated to the unit-cell volume evolution. Versus silicon content, the volume increase upon carbonation is reduced. The relative volume augmentation, $\Delta V/V$, varies from 5.05% for $x = 0.25$ down to 3.7% for $x = 1$. This effect suggests a reduction of the magnetic anisotropy field with increasing Si content, which is consistent, too, with the magnetic moment increase at 90 kOe and 5 K.

The maximum observed for coercivity as a function of T_A (Fig. 7) is a consequence of two opposing influences. Too low an annealing temperature hinders the complete solid-state reaction from forming a perfect metastable $Sm(Fe,Si)_9C$ phase, which is responsible for magnetic hardening. When increasing T_A, on the one hand, the number of surface defects of the hexagonal $P6/mmm$ phase is reduced, resulting in an increase of H_C; on the other hand, the x-ray diffraction domain size increases and reduces H_C.

HRTEM images were taken to study the morphology and the structure of three specific samples. The measurement of interplanar distances permits identification of the grains via their crystallographic parameters. Figure 8(b) is relative to grains of $SmFe_{8.75}Si_{0.25}C$, which exhibits the best coercivity for $T_A = 750$ °C. Figure 8(a) concerns the lowest $T_A = 650$ °C relevant for the smallest grain size around 10 nm and $H_C = 1.4$ kOe. Figure 8(c) corresponds to the highest $T_A = 1150$ °C with grain size around 40 nm and consistent with the $R\bar{3}m$ 2/17 structure and $H_C = 0.8$ kOe. Figure 8(b) represents the case of the optimal H_C equal to 15 kOe (Fig. 6). The grain size is around 22 nm, in agreement with the Rietveld analysis. The grain boundaries appear to connect the neighboring $P6/mmm$ grains without any intergranular layer and might favor the magnetic exchange coupling between the grains. The small remanence ratio M_r/M_s enhancement around 0.6 might be explained by intergranular exchange of grains of the main phase rather than via the grains belonging to the small iron contribution found by x-ray analysis and Mössbauer spectroscopy. The same trend for the remanence ratio is observed for all other compositions. They do not exhibit any free iron.

It must be outlined that the $R\bar{3}m$ alloys have been usually studied for the particular value $y = 2$ and two C atoms per unit formula 2/17, consistent with $x = 1$ and one C atom per unit formula 1/9. This Si composition seems here to be less

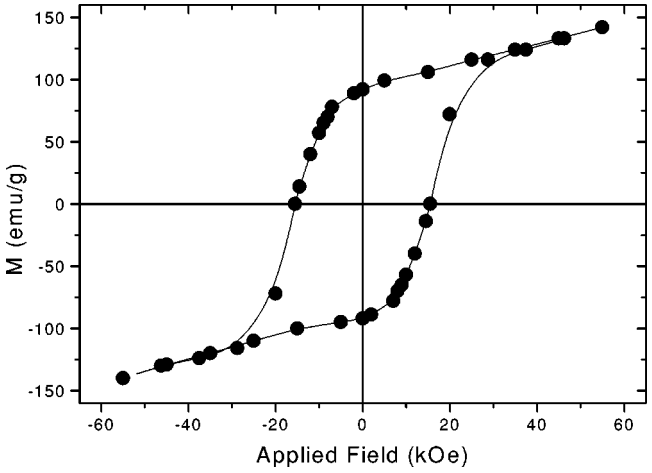

FIG. 6. Hysteresis loop at room temperature of $SmFe_{8.75}Si_{0.25}C$ annealed at 750 °C before carbonation.

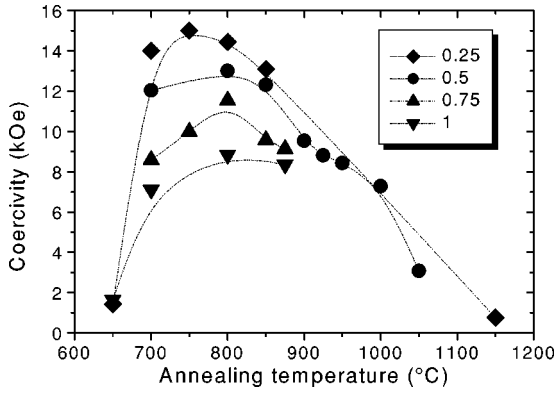

FIG. 7. Coercive field of carbides, at room temperature, vs annealing temperature of $Sm(Fe_{1-x}Si_x)_9$ for indicated x values.

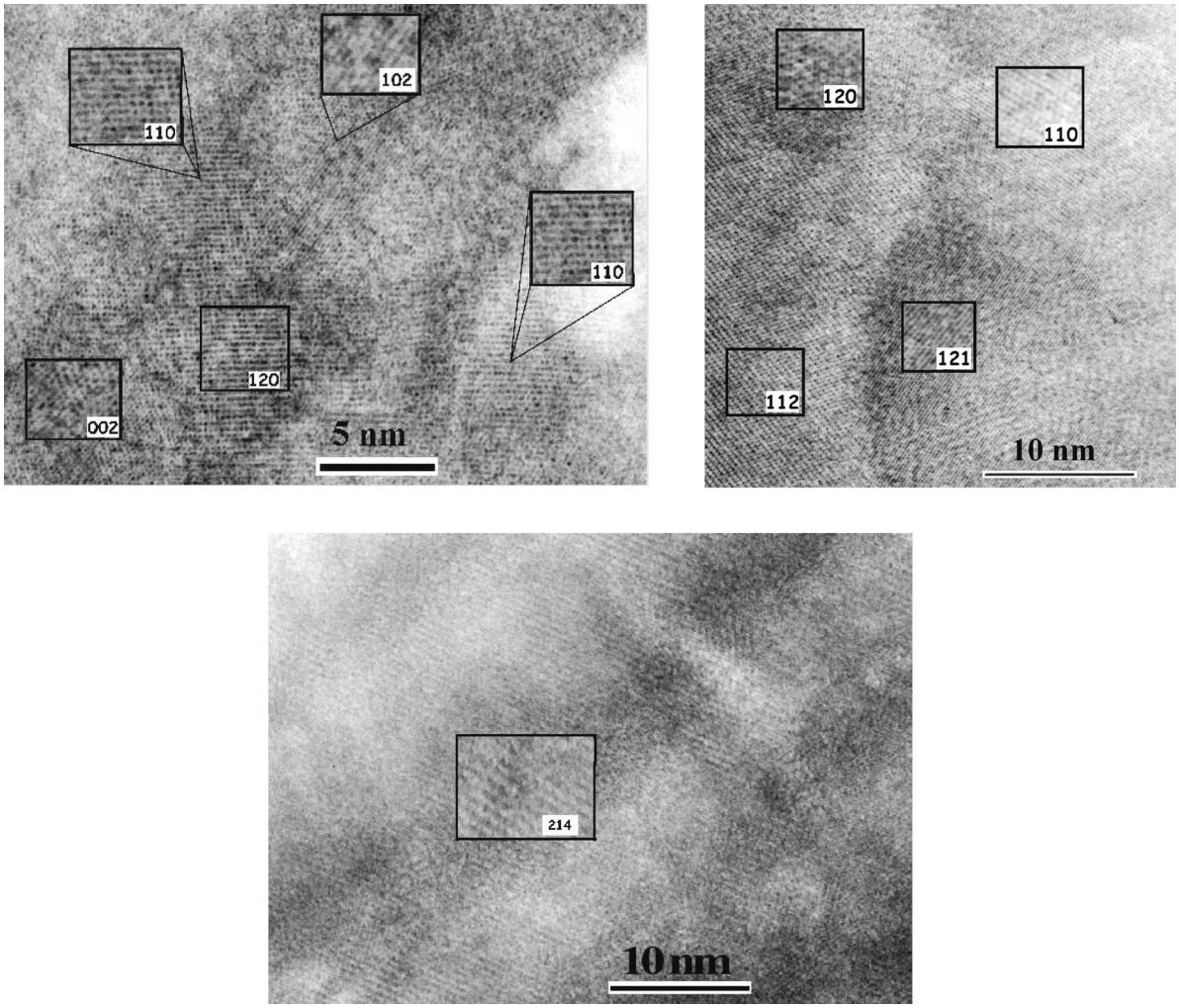

FIG. 8. High-resolution TEM image of grains of $SmFe_{8.75}Si_{0.25}C$. (a) Sample annealed at $T_A = 650$ °C. (b) Sample annealed at $T_A = 750$ °C. (c) Sample annealed at $T_A = 1150$ °C. In the insets higher magnifications of crystalline areas exhibit several sets of fringes.

efficient owing to a probable reduction of the anisotropy field. The high coercivity achieved in the mechanically alloyed magnet originates from the contribution of the metastable phase $Sm(Fe,Si)_9C$ rather than from that of $Sm_2(Fe,Si)_{17}C_2$. For the $P6/mmm$ 1/9 alloys, the composition $x = 0.25$ seems optimal but the alloys with Si content equal to 0.5 show still important H_C, with the advantage for a better thermal stability brought by the Si substitution.

IV. CONCLUSIONS

To the best of our knowledge, interstitial modification of $SmFe_{9-x}Si_x$ alloys ($0.25 \leqslant x \leqslant 1$) by carbonation with one carbon per unit formula has been carried out for the first time.

Carbonation leads to an expansion of the $P6/mmm$ crystal lattice. The Rietveld refinements point out individual unit-cell parameter evolutions, which corroborate the trend observed on the noncarbonated alloys. For the small Si contents $0.25 \leqslant x \leqslant 0.5$, a is reduced and c remains quasiconstant. For $x > 0.5$, the a decrease is partially balanced by the c increase and gives evidence for the small Fe stoichiometry enrichment of the $SmFe_9$ phase. It follows that the unit-cell expansion is reduced with x increasing.

The Curie temperature values of the carbonated 1/9 series are higher than those of the noncarbonated alloys, in agreement with the magnetovolume effect. These values are systematically raised compared to those of the homologous ordered $R\bar{3}m$ alloys (26 to 70 K). The average magnetic moment per iron atom, at 90 kOe and 5 K, increases with x as that of the noncarbonated alloys but remains smaller owing to the fact that carbon induces high anisotropy.

Because of the good resolution of the Mössbauer spectra, it was possible to perform a detailed analysis, based on the local environment of each of the three iron sites and on the effect of silicon and carbon on the structure and magnetic properties. The spectra were fitted accounting for the possible α-Fe contribution besides the main $SmFe_{9-x}Si_xC$ phase as suggested by x-ray diffraction. The amount of Fe equal to 6% wt for $x = 0.25$ is not detected for higher x content. This result gives evidence for the stabilizing effect of Si upon the $SmFe_9C$ alloys.

The interpretation of the $P6/mmm$ contribution to the Mössbauer spectra is based on the one hand on the binomial

distribution law of the Fe $2e$ dumbbells and the statistical occupation of Si on $3g$ site and, on the other hand, on the assignment of the various crystalline site isomer shifts δ according to the relationship between δ and the Wigner-Seitz cell volumes (WSC). The WSC volumes were calculated by means of a specific computing code with the use of the $P1$ group allowing the splitting of the partial Si and dumbbell occupation. It results the following sequence: $\delta\{2e\} > \delta\{3g\} > \delta\{6l\}$.

The specific $3g$ site behavior corroborates the preferential occupation of silicon at this site. The isomer shift increase of each individual crystallographic site is connected to the decrease of Fe s electron density with C insertion more pronounced for $3g$ and $6l$ atoms than for $2e$ atoms which have no C near neighbor. This increase reflects in fact the rare-earth $6s$ orbital charge transfer into the C atoms coupled to the volume expansion. Moreover the increase of the weighted average isomer shift, lower in carbides than in nitrides, attests for hybridization between $2p$ electrons of the interstitial element and $3d$ iron, stronger in carbides than in nitrides.

The hyperfine field sequence $H_{HF}\{2e\} > H_{HF}\{6l\} > H_{HF}\{3g\}$ agrees with the mean number of Fe near neighbors. The decrease of the mean hyperfine field results from the competition between the negative core polarization term and the positive $4s$ conduction term.

The high coercivity measured in these mechanically alloyed magnets is brought about by the $P6/mmm$ precursor $Sm(Fe,Si)_9C$ rather than by the $R\bar{3}m$ $Sm_2(Fe,Si)_{17}C_2$. Coercivity measured at 55 kOe at room temperature versus the annealing temperature of the noncarbonated alloys exhibits a maximum. The best coercivity of 15 kOe is observed for $x = 0.25$ for the annealing temperature of 750 °C and grain size around 22 nm as observed by high-resolution transmission electron microscopy and in agreement with the Rietveld fits. A small remanence ratio enhancement around 0.6, measured for all alloys, might result from intergranular exchange coupling between grains of the main phase more than from the free iron detected only for $x = 0.25$. The high coercivity of 13 kOe achieved for $x = 0.5$ makes this alloy still suitable for permanent-magnet application as it presents a better thermal stability.

ACKNOWLEDGMENTS

The authors are grateful to Dr. V. Lalanne for her technical help in the sample elaboration and wish to thank P. Beaunier (Service central de microscopie électronique de l'université Paris VI) for the HTREM micrographs.

[1] J.M.D. Coey and H. Sun, J. Magn. Magn. Mater. **87**, L251 (1990).
[2] C.N. Christodoulou and T. Takeshita, J. Alloys Compd. **198**, 1 (1993).
[3] O. Mao, Z. Altounian, J. Yang, and O. Strom-Olsen, J. Appl. Phys. **79**, 5536 (1996).
[4] X.P. Zhong, R.J. Radwanski, F.R. de Boer, T.H. Jacobs, and K.H.J. Buschow, J. Magn. Magn. Mater. **88**, 1 (1990).
[5] X.C. Kou, R. Grossinger, T.H. Jacobs, and K.H.J. Buschow, J. Magn. Magn. Mater. **86**, 333 (1990).
[6] H.W. Zhang, S.Y. Zhang, B.G. Shen, and L.G. Zhang, J. Appl. Phys. **83**, 4838 (1998).
[7] Z.W. Li, X.Z. Zhou, and A.H. Morrish, J. Phys.: Condens. Matter **6**, L283 (1994).
[8] L.X. Liao, X. Chen, Z. Altounian, and D.H. Ryan, Appl. Phys. Lett. **60**, 129 (1992).
[9] A. Handstein, M. Kubis, L. Cao, B. Gebel, and K.H. Muller, J. Magn. Magn. Mater. **192**, 281 (1999).
[10] M. Kubis, D. Eckert, B. Gebel, K.H. Muller, and L. Schultz, J. Magn. Magn. Mater. **217**, 14 (2000).
[11] O. Mao, J.O. Strom-Olsen, Z. Altounian, and J. Yang, J. Appl. Phys. **79**, 4605 (1996).
[12] L. Schultz, K. Schnitzke, J. Wecker, M. Katter, and C. Kuhrt, J. Appl. Phys. **70**, 6339 (1991).
[13] B.G. Shen, F.W. Wang, L. Kong, L. Cao, and W.S. Zhan, J. Appl. Phys. **75**, 6253 (1994).
[14] Y.Z. Ren, W.Y. Lee, C.D. Qin, D.H.L. Ng, and X.Y. Ma, J. Appl. Phys. **85**, 4672 (1999).
[15] B. Liang, B. Shen, Z. Cheng, H. Gong, J. Zhang, F. Wang, S. Zhang, and W. Zhan, J. Alloys Compd. **226**, 65 (1995).
[16] Z.W. Li and X.A.H. Morrish, J. Appl. Phys. **81**, 4545 (1997).
[17] W. Tang, Z.Q. Jin, J.R. Zhang, S.Y. Zhang, and Y.W. Du, J. Appl. Phys. **82**, 5054 (1997).
[18] C. Djéga-Mariadassou, L. Bessais, A. Nandra, J.M. Grenèche, and E. Burzo, Phys. Rev. B **65**, 014419 (2001).
[19] C. Djéga-Mariadassou, L. Bessais, A. Nandra, and E. Burzo, Phys. Rev. B **68**, 024406 (2003).
[20] L. Bessais, S. Sab, C. Djéga-Mariadassou, and J.M. Grenèche, Phys. Rev. B **66**, 054430 (2002).
[21] L. Bessais and C. Djéga-Mariadassou, Phys. Rev. B **63**, 54 412 (2001).
[22] M. Abdellaoui and E. Gaffet, Acta Metall. Mater. **43**, 1087 (1995).
[23] R. Vert, Ph.D. thesis, Université de Grenoble, 1999 (unpublished).
[24] H.M. Rietveld, Acta Crystallogr. **22**, 151 (1967).
[25] H.M. Rietveld, J. Appl. Crystallogr. **2**, 65 (1969).
[26] J. Rodríguez-Carvajal, Physica B **192**, 55 (1993).
[27] J. Rodríguez-Carvajal, M.T. Fernandez-Diaz, and J.L. Martinez, J. Phys.: Condens. Matter **3**, 3215 (1991).
[28] K.H.J. Buschow and A.S.V. der Goot, J. Less-Common Met. **14**, 323 (1968).
[29] M.Z. Huang, W.Y. Ching, and Z.Q. Gu, J. Appl. Phys. **81**, 5112 (1997).
[30] E.T. Teatum, K.A. Gschneidner, and J.T. Waber, *Rep. LA-4003* (Los Alamos Scientific Lab, Los Alamos, NM, 1968).
[31] B.P. Hu, H.S. Li, H. Song, and J.M.D. Coey, J. Phys.: Condens. Matter **3**, 3983 (1991).
[32] D.L. Williamson, S. Bukshpan, and R. Ingalls, Phys. Rev. B **6**, 4194 (1972).
[33] T. Beuerle and M. Fähnle, Phys. Status Solidi A **174**, 257 (1992).